buildings

MDPI

Article

Shear Strengthening of Full-Scale Precast Concrete Box Culvert Using Bonded FRP Panel

Taewon Ko [1], Song Choi [2], Sanghyeon Cho [1,*] and Wonseok Chung [1,*]

[1] Department of Civil Engineering, Kyung Hee University, 1732 Deogyeong-daero, Giheung-gu, Yongin-si 17104, Gyeonggi-do, Republic of Korea; taewon.ko@khu.ac.kr
[2] Seyeon Inc. Co., Ltd., C-1319, 26 Beobwon-ro 9-gil, Seoul 05836, Republic of Korea; songchoi0617@naver.com
* Correspondence: 0107sanghyun@khu.ac.kr (S.C.); wschung@khu.ac.kr (W.C.); Tel.: +82-31-201-2550 (W.C.)

Abstract

The shear capacity of underground box culverts decreases with increasing service life. Removing the soil above and enlarging the section are restricted. Bonded fiber-reinforced polymer (FRP) strengthening is suitable for these conditions, but full-scale verification remains limited. For this reason, the shear performance of a box culvert strengthened with an FRP panel was analyzed in full-scale tests. The initial cracking load increased to three times that of the control test unit. The deflection at the ultimate load decreased by 50.4%. The yield load of the steel reinforcement in the wall increased by 38%. A nonlinear finite element model predicted the initial cracking and ultimate loads with an error of no more than 4%. A parametric study was conducted on the concrete compressive strength, the panel thickness, and the strengthening of the haunches. As a result, the ultimate load decreased by only 21.5% when the compressive strength was lowered from 35 MPa to 15 MPa. A thicker panel mainly increased the initial cracking load, whereas extending the panel across the haunches increased the ultimate load by 4.6%. Bonded FRP strengthening improves the shear performance of a box culvert and remains effective in deteriorated concrete.

Keywords: precast concrete box culvert; bonded FRP strengthening; FRP panel; full-scale test; finite element analysis

1. Introduction

Underground box culverts are widely used as crossing structures beneath roads and railways. These box culverts carry both the upper soil fill and live loads [1,2]. In structures with a long service life, the shear capacity decreases owing to material deterioration and repeated loading. However, removing the soil above an underground box culvert is difficult because of the facilities on the surface and the need for traffic control. In addition, the space inside the box culvert is too limited to enlarge the section.

Bonded fiber-reinforced polymer (FRP) strengthening is suitable for these conditions because this method reduces the inner cross-section only slightly. Strengthening methods using FRP have been extensively verified for beam members [3–6]. Lee et al. [3] proposed a shear strength model for RC beams strengthened with externally bonded FRP and verified the model with the test results of 227 beams. Razaqpur et al. [7] confirmed that the debonding load increased by 46% when an externally bonded CFRP laminate was provided with mechanical anchorage. However, such strengthening efficiency is limited by debonding at the bond interface. Anchorage details and plate length determine this

Check for updates

Academic Editors: Aliakbar Gholampour, Naozumi Teramoto and Doo Yeol Yoo

Received: 2 October 2026
Revised: 20 October 2026
Accepted: 21 October 2026
Published: 25 October 2026

Copyright: © 2026 by the authors. Licensee MDPI, Basel, Switzerland. This article is an open access article distributed under the terms and conditions of the Creative Commons Attribution (CC BY) license.

limit [8,9]. The influence of anchorage conditions has also been confirmed for the near-surface mounted (NSM) method [10]. Applications to closed sections such as tunnels and pipelines have likewise been documented [11–13]. However, most existing studies on FRP strengthening have addressed simply supported beams or circular sections. Full-scale verification for a closed rigid-frame structure is limited to isolated cases such as the strengthening of a box culvert with precast segments [14]. Although the general design of externally bonded FRP strengthening is specified in the relevant guidelines [15,16], box culverts are not included within the scope of these guidelines.

Studies on box culverts have focused on the transfer of earth pressure and live load [17,18]. Garg et al. [17] measured the shear capacity of precast box culverts in full-scale tests. Ghahremannejad and Abolmaali [18] evaluated the same capacity by finite element analysis. The influence of haunch geometry and of internal glass FRP (GFRP) reinforcement used in place of steel reinforcement has also been examined [19,20]. These GFRP bars are cast into the box culvert during manufacture and are therefore restricted to new construction. For an existing box culvert, He et al. [21] inserted a glass fiber pipe and filled the gap with grout, achieving an increase in the ultimate load of approximately 67%. This method enlarges the section at the inner surface, whereas bonded FRP strengthening acts together with the existing section as a single unit with almost no reduction in the inner cross-section. Post-installed headed shear reinforcement has also been used for existing members [22], but unlike bonded FRP strengthening attached to the inner surface, this method requires drilling holes through the existing section. Full-scale verification of bonded FRP strengthening applied to a box culvert is therefore still needed. Table 1 compares this study with previous studies on the strengthening of box culverts.

Table 1. Comparison of this study with previous studies.

Study	Specimen	Strengthening Method	Approach	Variables
Wang et al. [14]	Full-scale box culvert	Precast segment liner	Field load test	Liner installation
He et al. [21]	Box culvert	Glass fiber pipe liner with grout	Test and FE analysis	Liner, interface bond
This study	Full-scale precast box culvert	Bonded FRP panel	Test, FE analysis, parametric study	Concrete strength, panel thickness, layout

The objective of this study is to evaluate the effect of bonded FRP strengthening on the shear performance of a box culvert. This study used full-scale tests to verify the strengthening performance of a method in which a 5-mm-thick FRP panel is bonded to the inner surface using epoxy and anchors. Two test units were fabricated as precast box culverts with an inner space of 2.0 m × 1.5 m. An eccentric uniformly distributed load was applied at a distance of one effective depth from the haunch to induce shear failure. The strengthening effect of the FRP panel was confirmed by comparing the load–displacement relationship, the strains in the main steel reinforcement, and the crack propagation pattern with and without strengthening. In the analysis, a three-dimensional nonlinear finite element model based on the concrete damaged plasticity (CDP) model was constructed from the test results, and the validity of the model was verified. Finally, a parametric study was performed using the verified model with concrete compressive strength, panel thickness, and strengthening method as variables.

2. Materials and Experimental Program

To evaluate the effect of bonded FRP strengthening on the shear performance of a box culvert, one control test unit and one strengthened test unit were fabricated from the same concrete batch. Each test unit was a precast box culvert with an inner space of 2.0 m × 1.5 m and a length of 1.0 m. The shape and dimensions of the test unit are presented in Figure 1. The slab and wall thicknesses were 180 mm and 160 mm, respectively. A 200 mm haunch was provided at each inner corner. The concrete mix was designed for a compressive strength of 35 Mpa, and SD400 steel reinforcement was used. The material tests showed a compressive strength of 37.3 ± 0.9 Mpa for the concrete and a yield strength of 428 ± 5 Mpa and a tensile strength of 567 ± 10 Mpa for the steel reinforcement. Figure 2 presents the steel reinforcement details in the front view (Figure 2a), the slab (Figure 2b), and the wall (Figure 2c).

Figure 3 details the arrangement and dimensions of the FRP panel in the front view (Figure 3a), the slab (Figure 3b), and the wall (Figure 3c). The panel combines structural plies and flame-retardant plies in one stack. A 5-mm stack is the thinnest that includes every functional ply. Coupon tests confirmed that the panel was a quasi-isotropic laminate with an elastic modulus of 41 Gpa, a shear modulus of 18.7 Gpa, and a tensile strength of 616 Mpa. To simplify installation, the panel was fabricated as separate plates. The plates were arranged on the bottom surface of the slab and the Inner surface of the wall.

The fabrication process of the test unit Is Illustrated In Figure 4. The steel reinforcement was first assembled in accordance with the design drawings (Figure 4a). Strain gauges were attached to the steel reinforcement (Figure 4b), after which the concrete was poured and moist-cured for 28 days (Figure 4c). After curing was completed, the inner surface of the test unit was smoothed, and the FRP panel was placed (Figure 4d). An epoxy resin with a tensile strength of 53.8 Mpa was injected between the panel and the concrete to form the bond interface. The epoxy layer was approximately 3 mm thick and was moist-cured for 14 days. After curing, anchors were inserted to provide mechanical anchorage for the panel (Figure 4e). A total of 32 anchors were arranged at 400-mm intervals. The anchors were M6 wedge anchors of the mechanical expansion type with an effective embedment depth of 40 mm and a characteristic resistance of 6 kN. The strengthened test unit completed through this process is presented in Figure 4f.

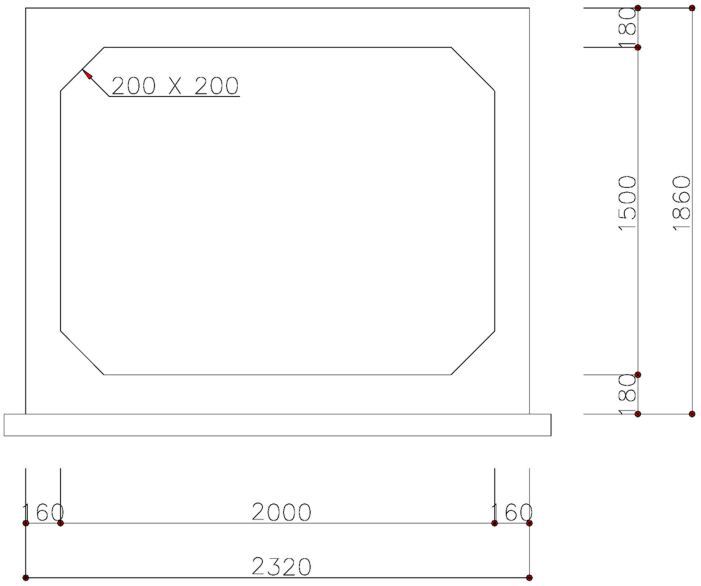


Figure 1. Dimensions of the precast concrete box culvert test unit.

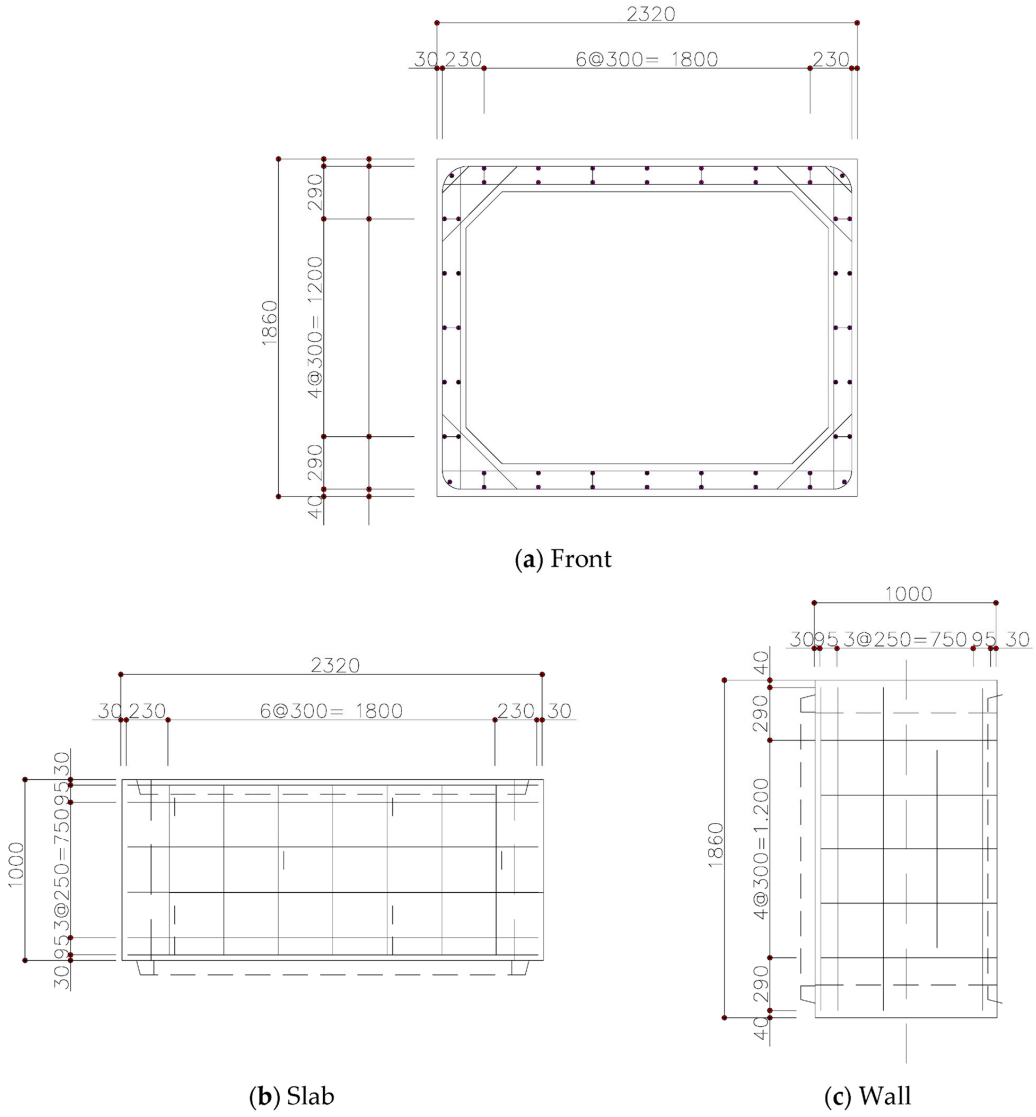


Figure 2. Details of precast concrete box culvert test unit.

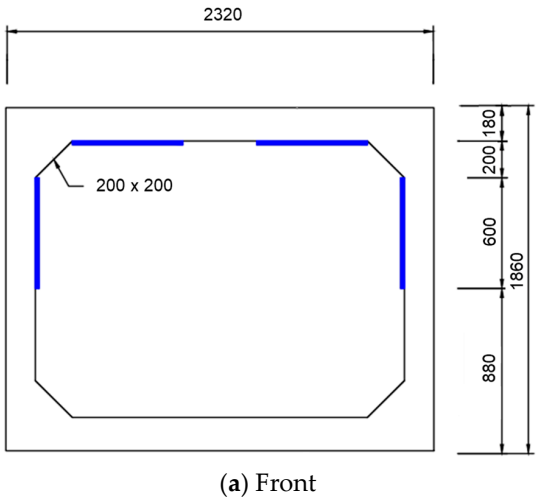
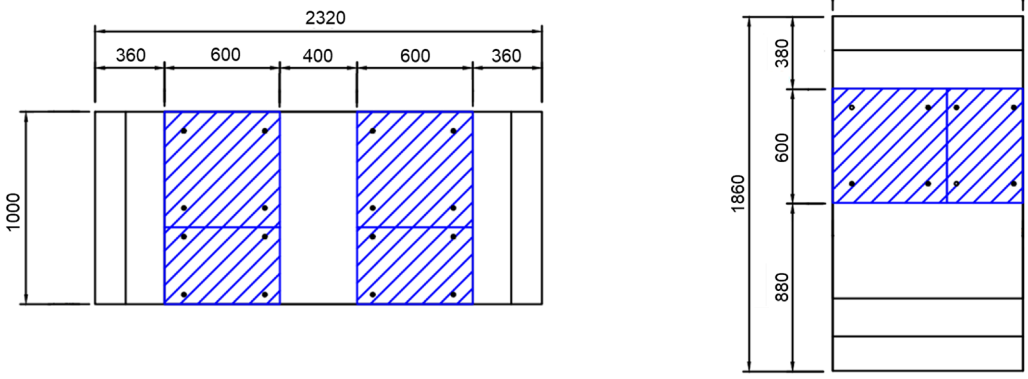


Figure 3. *Cont.*



(**b**) Slab (**c**) Wall

Figure 3. Dimensions of bonded FRP panel.



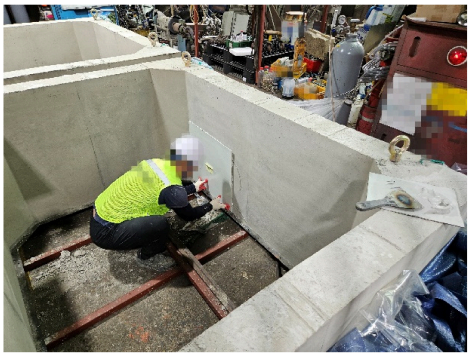
(**a**) Assembling steel reinforcement



(**b**) Setting sensor



(**c**) Pouring and curing concrete



(**d**) Attaching FRP panel



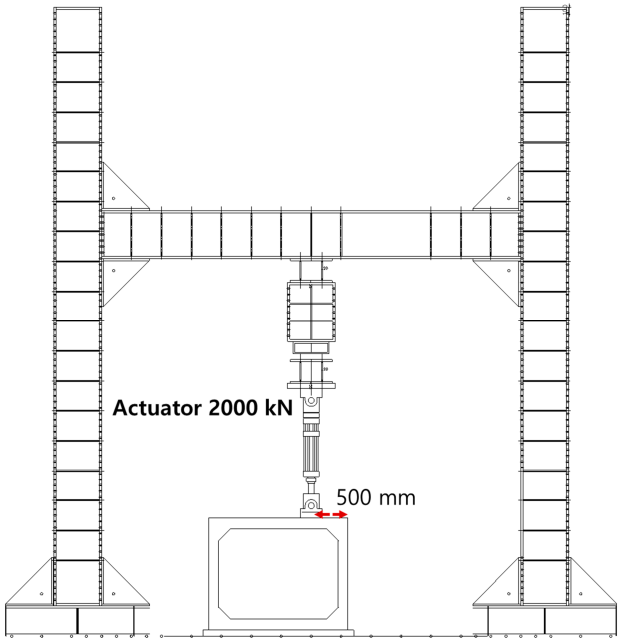
(**e**) Injecting epoxy and inserting anchor



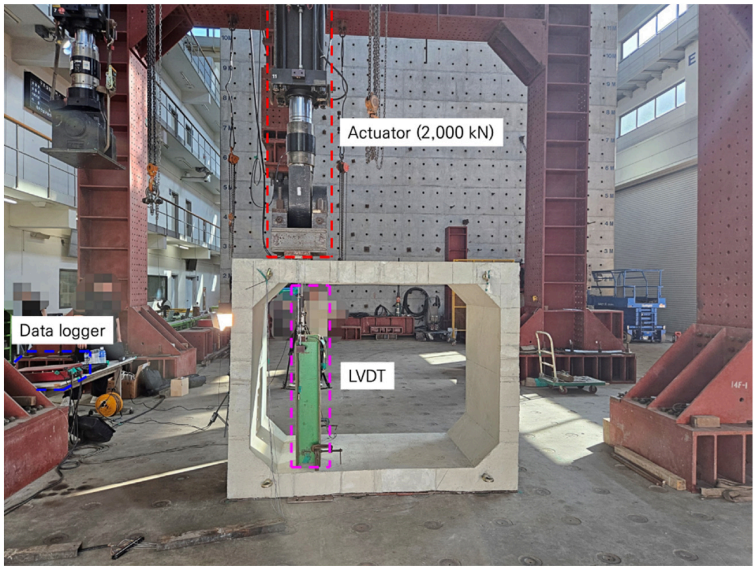
(**f**) Completion of test unit

Figure 4. Fabrication of test unit.

Figure 5 illustrates the load and boundary conditions of the loading test (Figure 5a) and a view of the test (Figure 5b). The test unit was placed directly on the concrete floor of the laboratory. The test was conducted using an actuator with an axial load capacity of 2000 kN. The load was applied through a steel plate of 200 mm along the span by 1000 mm across the full width. The center of the loaded area lay at a distance of one effective depth from the haunch, the position that places the highest shear demand on the section. Loading was performed under displacement control at a rate of 0.03 mm/s. Under load control, abrupt deformation occurs immediately after the ultimate load is reached, and the post-failure behavior is therefore difficult to capture. In contrast, displacement control maintains a constant loading rate and allows crack propagation and the failure pattern to be observed stage by stage. For this reason, displacement control is generally adopted for analyzing the failure modes of concrete structures [23], and the same method was applied in this study.



(**a**) Load and boundary condition



(**b**) Test view

Figure 5. Test set-up.

The measurement sensors were attached at the locations indicated in Figure 6. A linear variable differential transformer (LVDT) was installed on the bottom surface of the slab directly beneath the loading point to measure the vertical deflection. The LVDT had a measurement range of 100 mm and a resolution of 0.01 mm, and electrical resistance strain gauges with a gauge length of 5 mm were used. Strain gauges were attached directly to the steel reinforcement before the concrete was poured. In the slab, the gauges were placed beneath the loading point, 500 mm from the outer face of the right wall. In the wall, the gauges were placed at the right part adjacent to the loading point, 930 mm above the base of the test unit. This height corresponds to half of the total height of the test unit (h/2, h = 1860 mm). Two strain gauges were attached at each location, and the average of the two readings was taken as the strain at that location. The yield load of the steel reinforcement was taken as the load at which this strain reached the yield strain of 2000 με. Cracks were visually inspected and marked at each load step, and the initial cracking load of each test unit was taken as the load at which the first crack was observed.

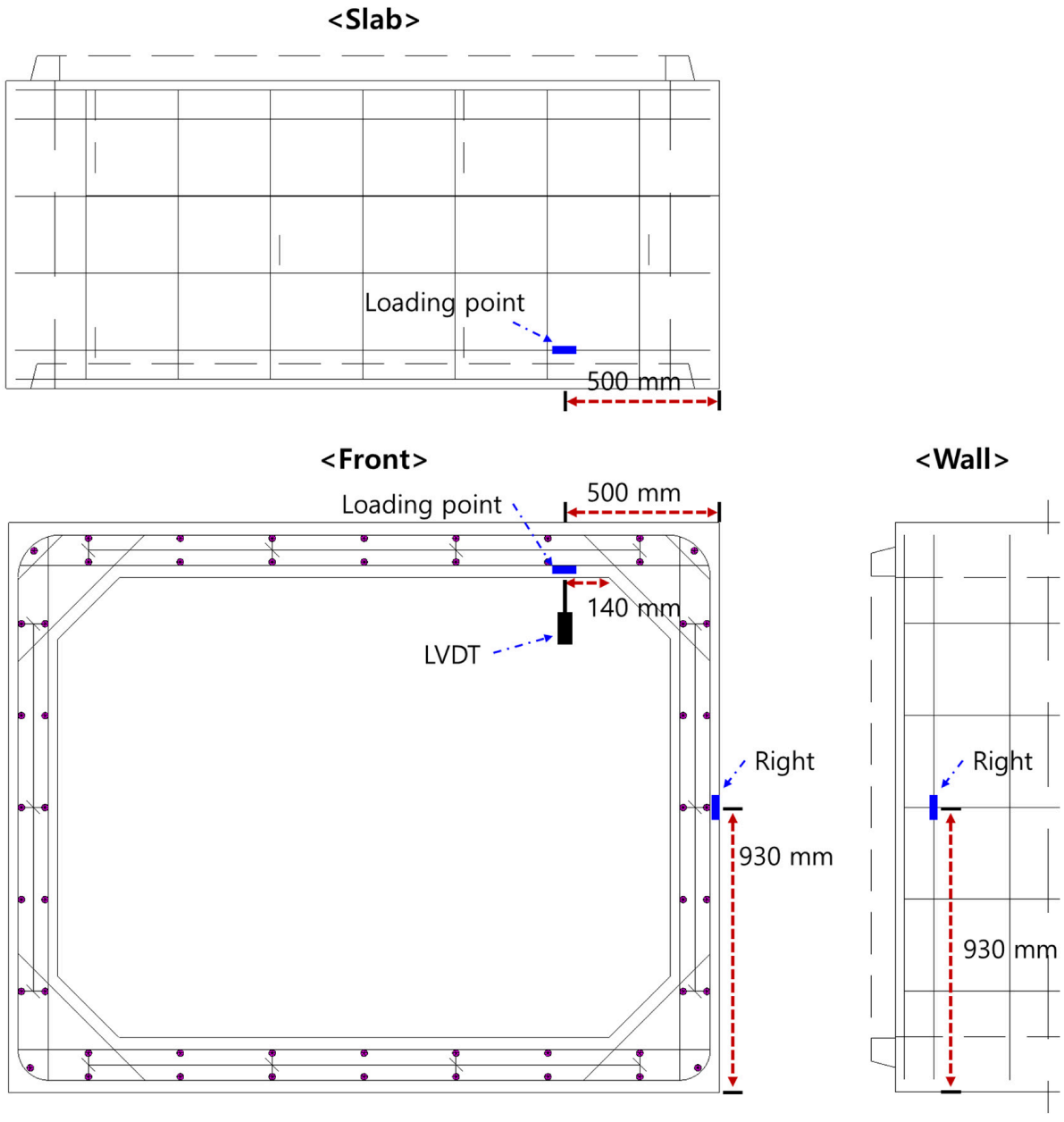


Figure 6. Locations of sensors on test unit.

3. Experimental Results

The load–displacement relationships with and without the FRP panel are compared in Figure 7. The initial cracking load of the strengthened test unit increased to three times that of the control test unit, from 50 kN to 150 kN. As defined in Section 2, both values are the loads at which the first crack was observed during the test. The strains in Figure 8 became nonlinear at the same loads, and the crack patterns in Figure 9 confirm this observation. The ultimate loads of 455.7 kN and 459.2 kN differed by only 0.8%. In contrast, the deflection at the ultimate load of each test unit decreased by 50.4% from 13.25 mm to 6.57 mm. The measured ultimate loads were 2.4 times the nominal strength of 188 kN, which was calculated from the slab shear equation of ACI 318-19 [24]. The nominal strength was obtained from $V_c = 0.17\sqrt{f'_c}b_w d$ with f'_c = 35 MPa, b_w = 1000 mm, and d = 140 mm (V_c = 140.8 kN) and was converted to the applied load using the ratio of the support reaction to the applied load of 0.75. The shear reinforcement was not included because the spacing of 300 mm exceeded d/2. The ultimate loads exceeded the nominal strength because the load was applied at a shear span-to-depth ratio of 1.0, at which the force passes to the wall through a direct compression strut that the sectional shear equation does not consider. Given that Ghahremannejad and Abolmaali [18] as well as Elnady et al. [20] also found shear capacities well above the code value for concrete box culverts, the ratio of 2.4 is considered reasonable. Overall, the FRP panel increased the initial cracking load and reduced the deflection, whereas the ultimate load remained almost unchanged.

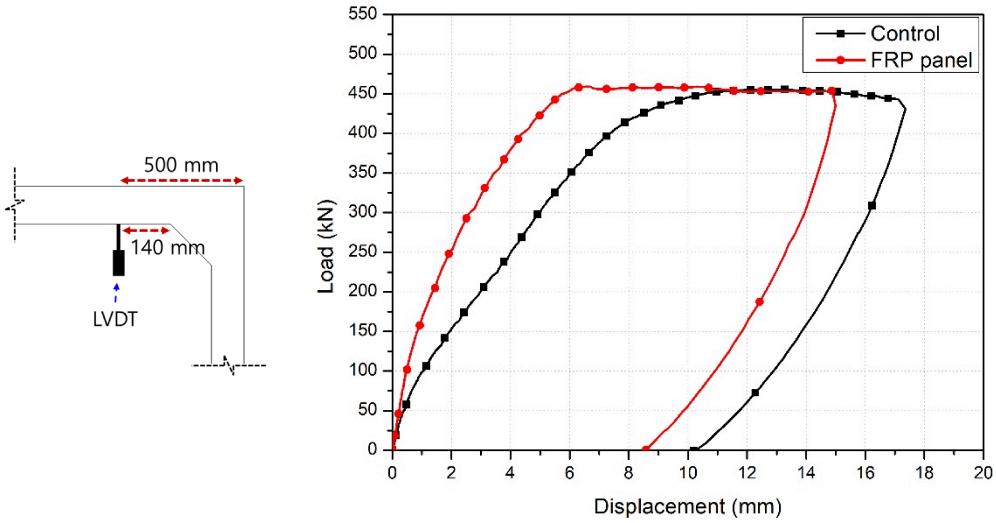
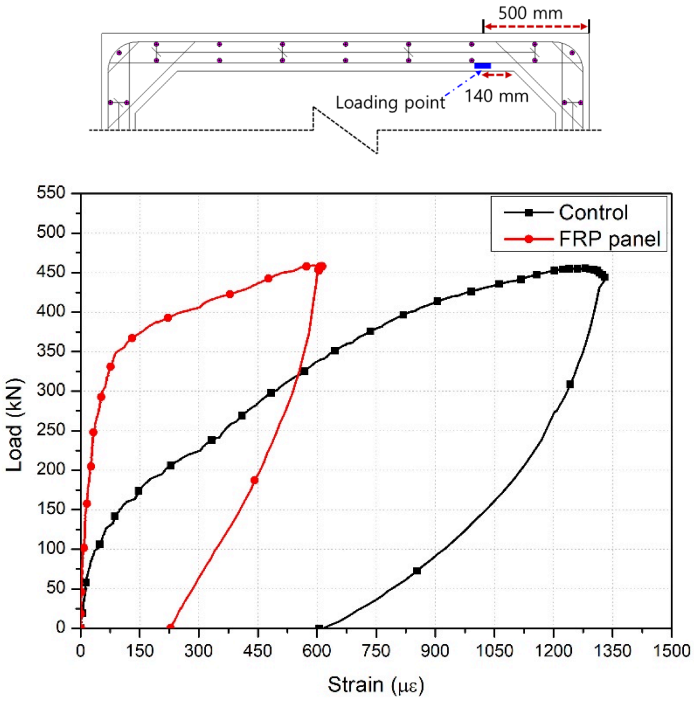


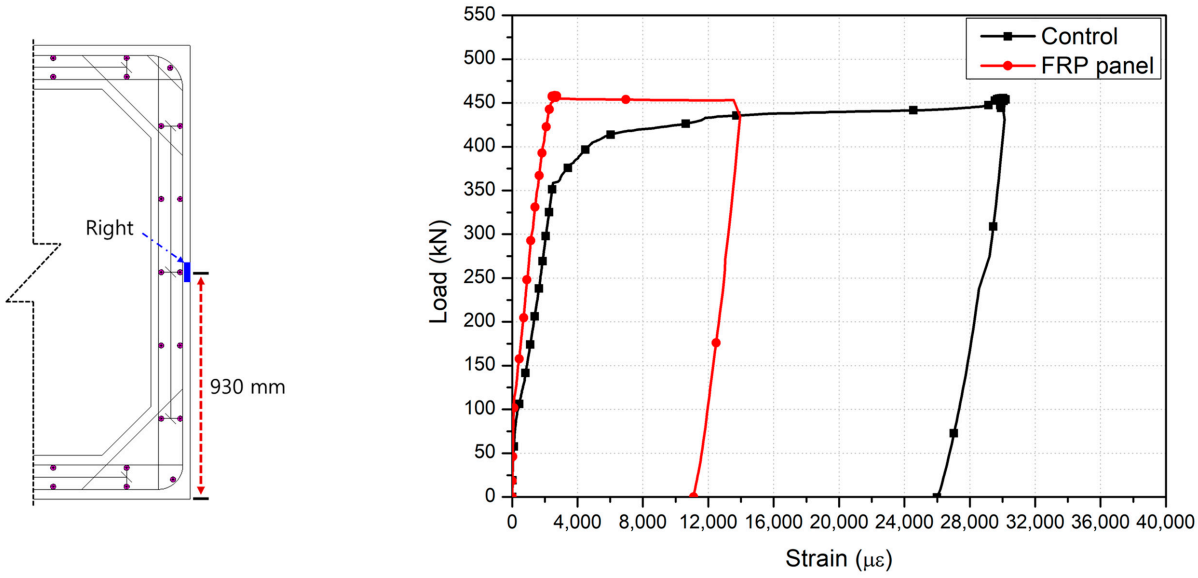
Figure 7. Displacement results with and without FRP panel.

Figure 8 compares the load–strain relationships at the loading point of the slab (Figure 8a) and at the right part of the wall (Figure 8b). At the loading point of the slab (Figure 8a), the strain of the control test unit became nonlinear at 50 kN owing to the initial cracking of the concrete. In the strengthened test unit, slight nonlinearity owing to initial cracking appeared at 150 kN. The nonlinearity increased at 350 kN with the propagation of the crack at the slab–haunch junction without the panel. The strain measured at the loading point did not reach the yield strain in either test unit. At the right part of the wall (Figure 8b), the steel reinforcement of the control test unit reached the yield strain at 300 kN. From 350 kN, the extension of the cracks in the wall intensified the nonlinear response. Beyond 400 kN, the strain exceeded 20,000 με, which indicates large plastic deformation of the steel reinforcement before the ultimate load. In the strengthened test unit, the wall strain deviated slightly from linearity at 150 kN owing to cracking. The yield load of the steel reinforcement at the right part of the wall was 414 kN in the strengthened test unit,

which is 38% higher than that of the control test unit. A distinct transition in the wall strain occurred at the ultimate load of 459.2 kN, when the concrete at the slab–haunch junction failed in shear. The strains of the steel reinforcement also confirmed the strengthening effect of the FRP panel.



(**a**) Loading point of slab



(b) Right part of wall

Figure 8. Strain results with and without FRP panel.

As shown in Figure 9, the crack patterns at 150 kN and at the ultimate load differed between the control test unit (Figure 9a) and the strengthened test unit (Figure 9b). In the control test unit (Figure 9a), initial cracks formed in the upper slab at 50 kN. As the load increased to 150 kN, the cracks concentrated in the slab adjacent to the haunch and around the haunch. A few cracks also formed on the outer face of the wall near the haunch.

In the strengthened test unit (Figure 9b), a single fine crack was observed at 150 kN in the unbonded region beyond the end of the FRP panel. At the ultimate load, horizontal cracks extended across the wall of the control test unit from the outer face to the inner face. The wall governed the failure of this test unit. In the strengthened test unit, the cracks in the wall were limited to the region near the haunch. Diagonal cracks developed at the junction between the upper slab and the haunch, which was cast monolithically and was not covered by the panel. The extension of these diagonal cracks governed the failure at 459.2 kN. In the strengthened test unit, cracks were observed on the surfaces not covered by the panel, including the side faces where the cross-section is exposed, and debonding was checked along the panel edges. Neither rupture of the FRP panel nor cracking between the panel and the concrete was observed. In both test units, the cracks and the failure concentrated in the corner region around the haunch rather than spreading along the span. The damage developed along the compression strut that carried the load directly from the loading area near the haunch to the wall. The FRP panel suppressed cracking on the bonded faces, whereas the ultimate load was governed by this strut and the slab–haunch junction without the panel.

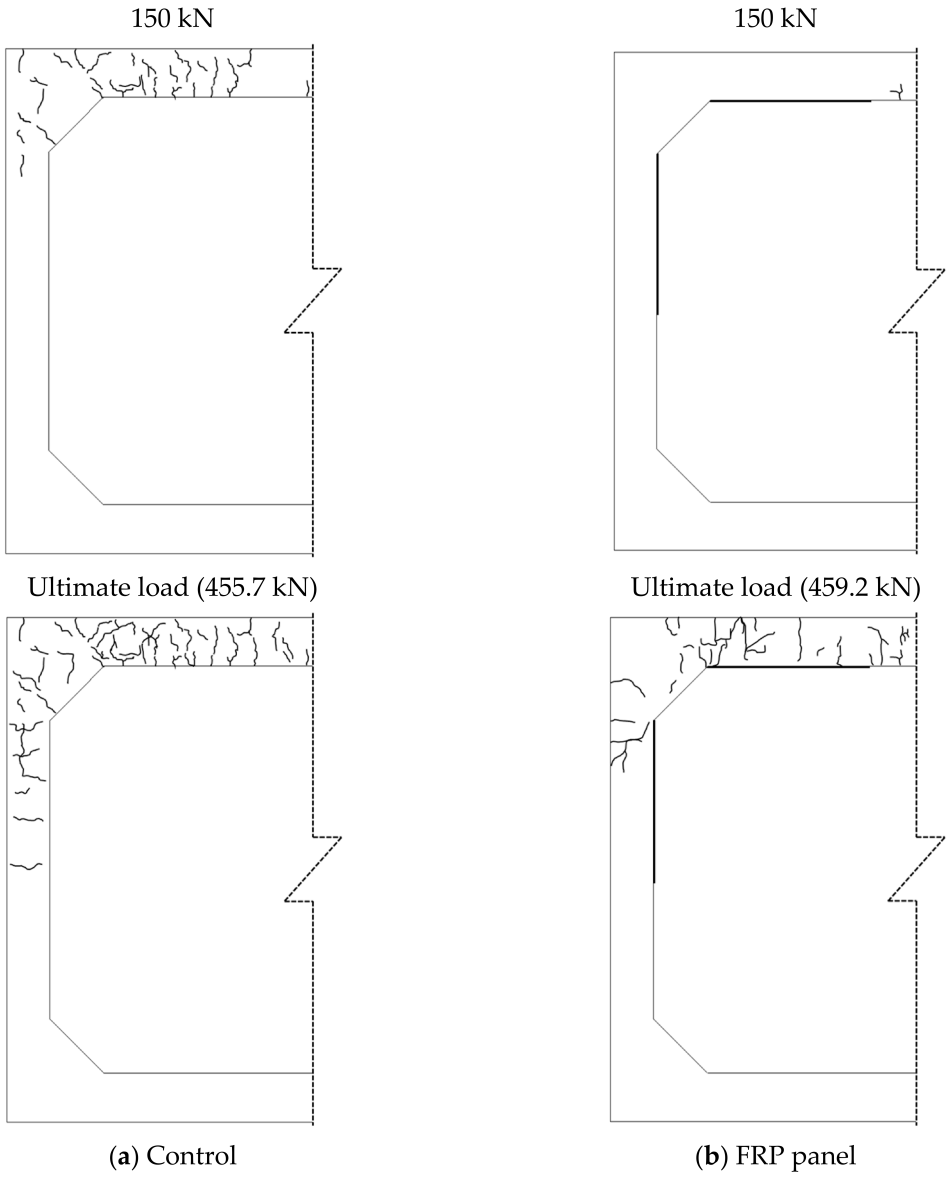


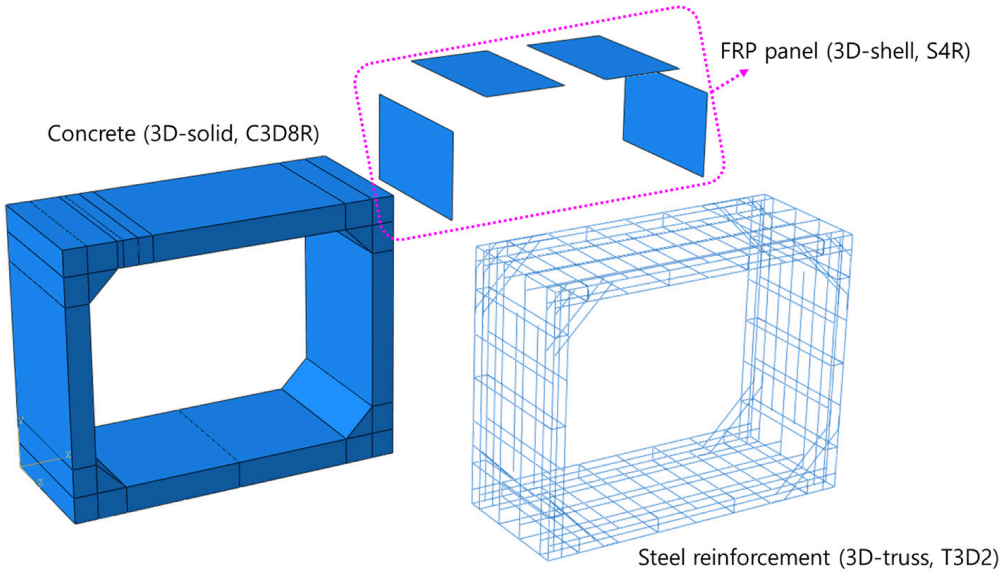
Figure 9. Crack pattern of test unit.

4. Finite Element Analysis

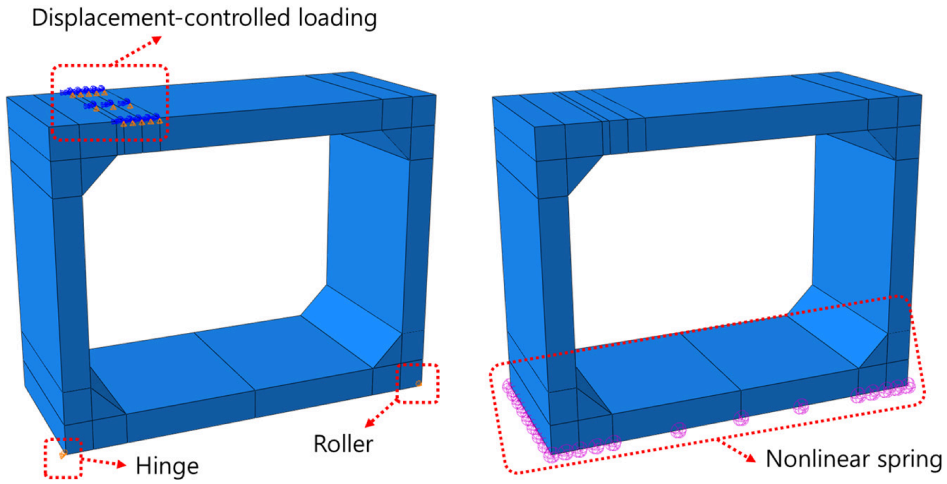
The finite element model was built to reproduce the measured behavior, to complement the single test for each condition, and to extend the results to conditions that the tests did not cover. The model represented the strengthened test unit, including the FRP panel, the epoxy bond interface, and the anchors, and the analytical results were compared with the measured results of this test unit. Figure 10 presents the element configuration (Figure 10a) and the load and boundary conditions (Figure 10b) of the constructed finite element model. The analysis was performed using the commercial program ABAQUS [25]. The concrete was modeled with reduced-integration solid elements (C3D8R). The steel reinforcement was modeled with two-node truss elements (T3D2) and was embedded in the concrete using an embedded element constraint. The FRP panel was modeled with four-node reduced-integration shell elements (S4R). The element size was approximately 50 mm for the concrete. Figure 11 compares the load–displacement relationships for element sizes of 50, 40, and 30 mm. The curves almost coincided up to the ultimate load, and the initial cracking load and the ultimate load differed by less than 3% from those of the 50 mm mesh. After the ultimate load, the load decreased slightly faster for the smaller element size because the damage localized in a narrower band. The element size of 50 mm was adopted considering the computational efficiency. The entire model consisted of 17,638 elements and 20,497 nodes. The epoxy bond interface was simulated with nonlinear connector elements linking the concrete surface and the panel. The connector elements were elastic in compression, and the normal tension and the shear force were limited to the tensile strength of the concrete and the bond strength, respectively, multiplied by the tributary area of each node. The anchors were likewise placed as nonlinear connector elements at the same locations as in the test. The boundary conditions were the same as in the test. The contact between the test unit and the floor was modeled with nonlinear spring elements that resist compression only. As in the test, the load was applied under displacement control by incrementally increasing the displacement at the loading point. The stiffness of concrete structures degrades abruptly near the ultimate load. When load control is applied, the analysis terminates in this range, which prevents identification of the failure mode. Displacement control maintains convergence and allows the behavior beyond the ultimate load to be traced. Displacement control was likewise adopted by Genikomsou and Polak [26] as well as Seręga and Kotynia [27]. Both studies analyzed the failure behavior of concrete structures and compared the results with tests.

The material nonlinearity of the concrete was defined using the CDP model [28,29]. The compressive strength of the concrete and the yield strength of the steel reinforcement were set to the design values of 35 MPa and 400 MPa, respectively, and the elastic modulus of the concrete was set to 27,800 MPa from the design equation of ACI 318-19 [24]. The CDP model has been widely applied to shear and punching analyses of reinforced concrete members [26,27]. The dilation angle, eccentricity, ratio of the biaxial to uniaxial compressive strength, ratio of the second stress invariants on the tensile and compressive meridians, and viscosity parameter were 34°, 0.1, 1.16, 0.67, and 0.000215, respectively. The compressive stress–strain relationship followed the unconfined concrete curve of Mander et al. [30]. In accordance with the fictitious crack concept [31–33], tension softening was defined in terms of the crack width using the bilinear curve of CEB-FIP [34,35]. The compressive damage variable increased from zero at the peak stress to 0.92, and the tensile damage variable was defined as a function of the crack width up to 0.90 [36–38]. The shear strength of the epoxy bond interface was taken from the value proposed by Lu et al. [39]. The steel reinforcement was defined as elastic–perfectly plastic. Because coupon tests confirmed that the FRP panel was a quasi-isotropic laminate, the panel was defined as an in-plane isotropic

elastic material that reproduces both the measured elastic modulus and the measured shear modulus.



(**a**) Part modeling



(**b**) Load and boundary conditions

Figure 10. Finite element model.

Figure 12 compares the load–displacement relationships of the strengthened test unit obtained from the test and from the analysis. The analysis predicted an initial cracking load of 154.0 kN, 2.7% above the measured value of 150 kN. The predicted ultimate load of 474.1 kN exceeded the measured 459.2 kN by 3.2%. Over the entire range, the analytical load exceeded the measured load by 3.0% on average. The boundary and connection conditions of the analytical model were stiffer than the actual conditions of the test unit, which explains the higher analytical load. The model predicted the initial cracking load and the ultimate load within 4% and is considered suitable for predicting the behavior of a box culvert with bonded FRP strengthening.

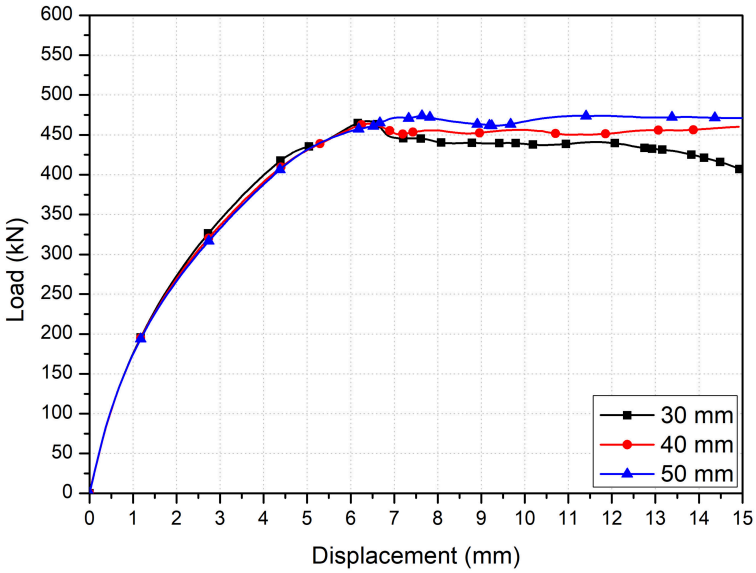


Figure 11. Load–displacement relationships according to element size.

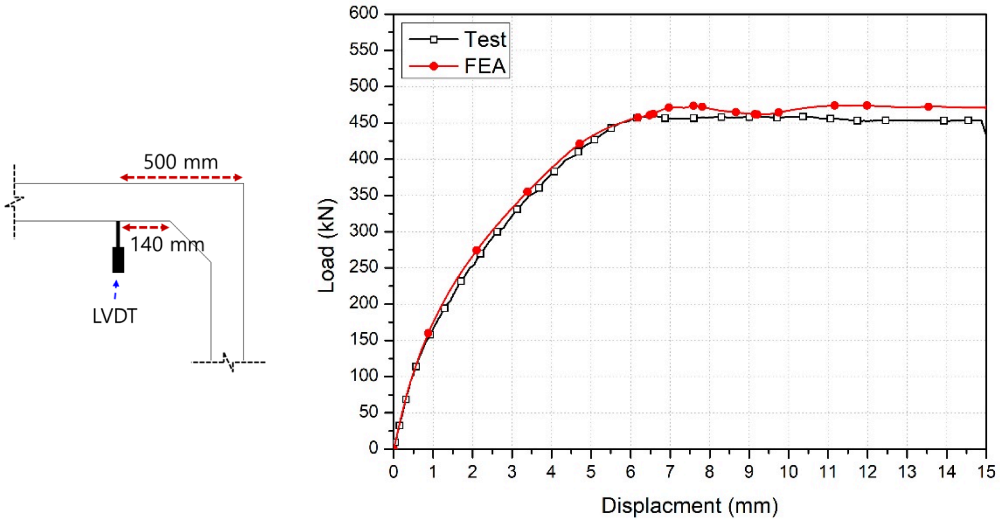
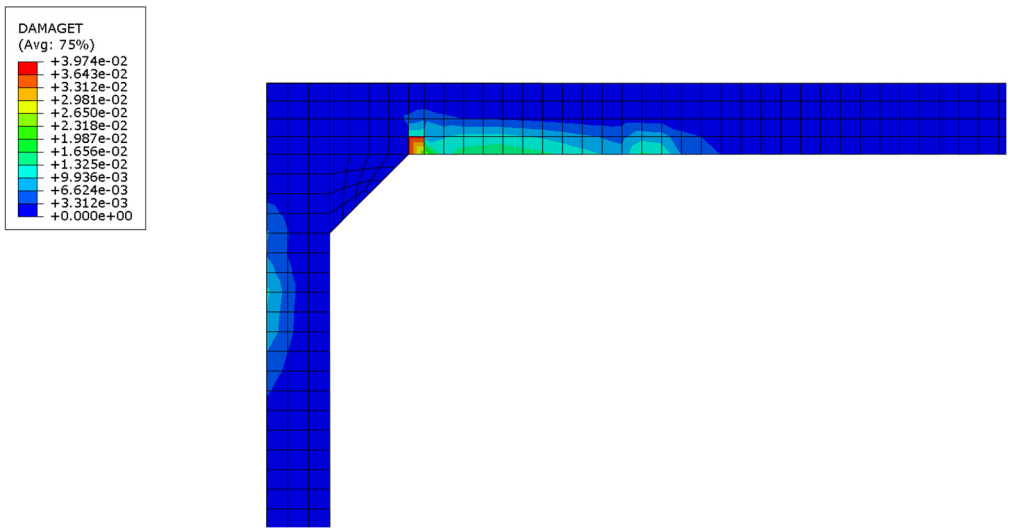
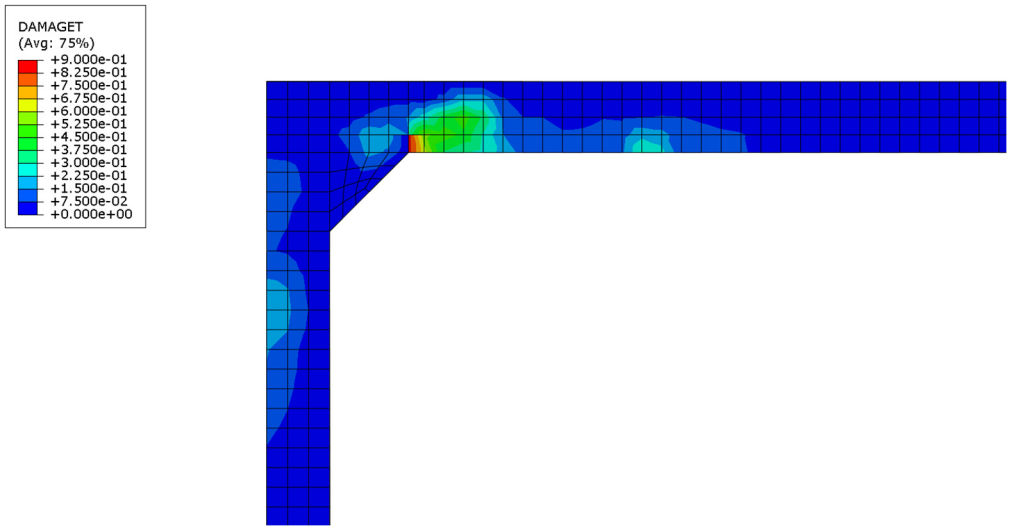


Figure 12. Load–displacement comparison between experimental results and finite element analysis.

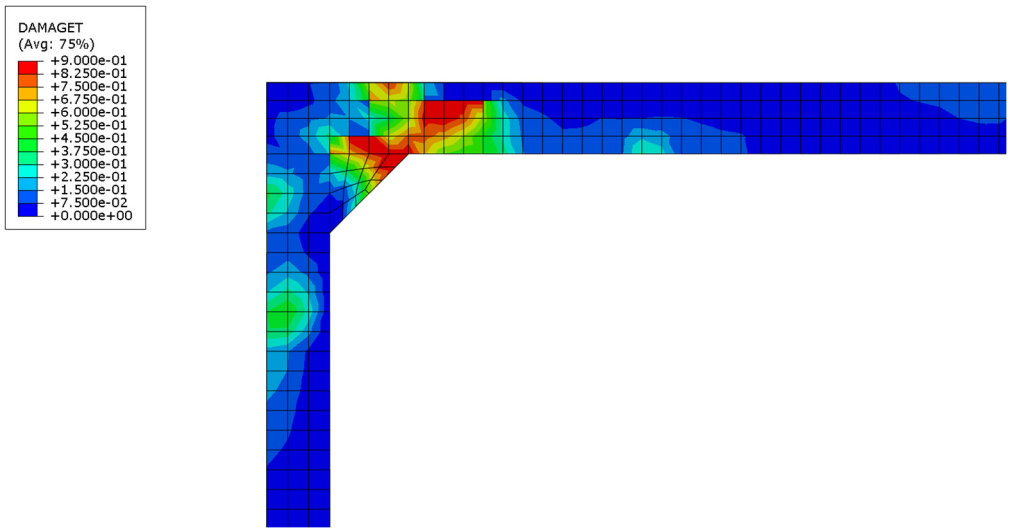
The tensile damage distribution of the finite element model at each load stage is visualized in Figure 13. Figure 13a is the stage at the initial cracking load (154.0 kN). At this stage, the tensile damage was limited to the bottom surface of the upper slab and to the slab–haunch junction. At the ultimate load of 474.1 kN (Figure 13b), the damage extended along the bottom surface of the upper slab near the haunch and appeared on the outer face of the wall. In the final damage pattern (Figure 13c), high damage concentrated in a diagonal band between the loading area and the haunch. The damage on the outer face of the wall also increased, whereas the slab beyond the loading area remained almost undamaged. These results confirm that the model captures the failure mechanism of a box culvert with bonded FRP strengthening, including the location of the critical diagonal crack.



(**a**) Initial cracking load (154.0 kN)



(**b**) Ultimate load (474.1 kN)



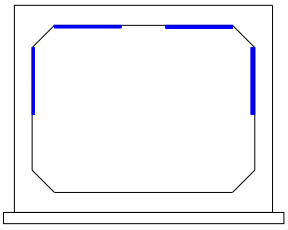
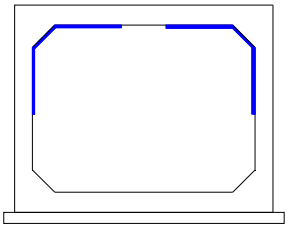
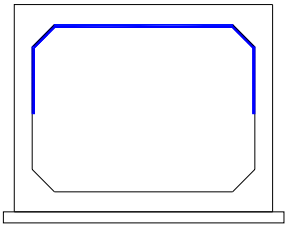
(**c**) Final damage pattern

Figure 13. Damage pattern predicted by finite element model.

5. Parametric Study

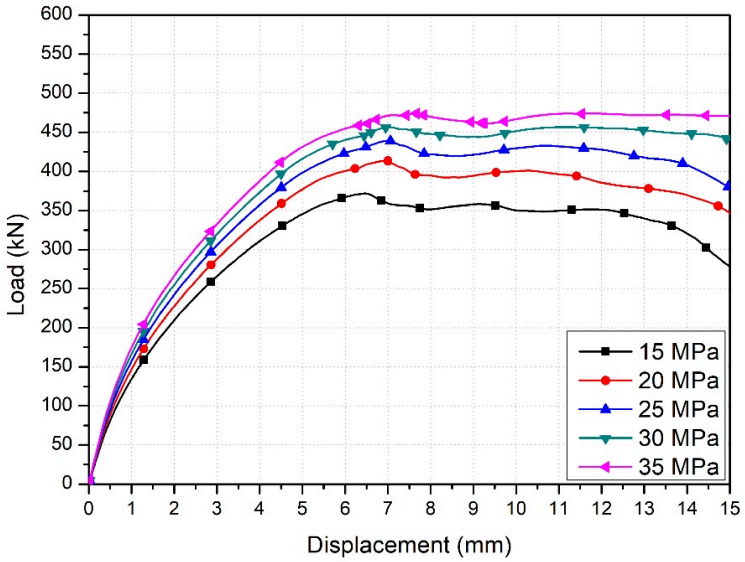
In the parametric study, the verified finite element model was used to examine the concrete compressive strength, the FRP panel thickness, and the strengthening method. The elastic modulus, tensile strength, and fracture energy were scaled with the compressive strength in accordance with ACI 318-19 [24] and the fib Model Code 2010 [35]. The properties of the steel reinforcement and the bond between the reinforcement and the concrete were kept constant. The lower bound of 15 MPa lies below the minimum substrate strength of 17 MPa specified in ACI 440.2R-17 [15] and was included as a parametric boundary. The panel thickness was increased from the tested 5 mm to 20 mm. The strengthening method was examined for the three cases in Table 2: the tested arrangement (case A), the panel extended across the upper haunches (case B), and the midspan gap also filled (case C). The reference case corresponded to the test unit (f_{ck} = 35 MPa, t = 5 mm, case A). In Figures 14b, 15b and 16b, the load variation on the vertical axis is the change in the initial cracking load or the ultimate load relative to the reference case, expressed as a percentage of the reference value. A positive value indicates an increase, and a negative value indicates a decrease. The same finite element model verified against the strengthened test unit was used in all cases. Only the examined variable was changed in each case, and the mesh, the boundary and loading conditions, the bond and anchor models, and the remaining material properties were kept identical to those of the verified model.

Table 2. Strengthening method of each case.

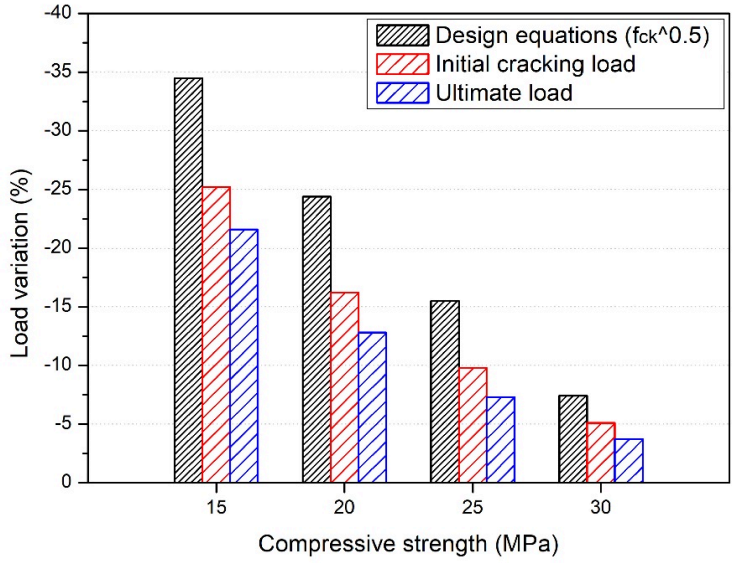
Case	Strengthening Location	Bonded Area (m^2)	Schematic
A	Slab (400 mm gap at midspan) + Wall	2.61	
B	Slab (400 mm gap at midspan) + Wall + Haunch	2.98	
C	Slab + Wall + Haunch	3.37	

The compressive strength was varied from 15 MPa to 35 MPa in 5 MPa steps with the panel thickness fixed at 5 mm. As shown in Figure 14a, lowering the compressive strength from 35 MPa to 15 MPa decreased the initial cracking load by 25.2% and the ultimate load by 21.5%. Figure 14b compares the reductions in the initial cracking load and the ultimate load with the reduction predicted by the design equations. The vertical axis gives the load variation relative to the reference case of 35 MPa and is reversed, so

that a larger reduction appears as a taller bar. In ACI 318-19 [24], the modulus of rupture associated with the initial cracking load and the concrete contribution to the shear strength associated with the ultimate load are both proportional to $\sqrt{f_{ck}}$. These equations predict a reduction of 34.5% in both the initial cracking load and the ultimate load over the same range. At each strength, the bar for the design equations gives the reduction predicted from the square root of the compressive strength. A bar for the initial cracking load or the ultimate load that is shorter than this bar indicates a smaller reduction than the prediction. Both loads fell below this prediction at every strength. The difference from the prediction increased as the compressive strength decreased (Figure 14b). Because the properties of the steel reinforcement and the FRP panel are independent of the compressive strength, these components limited the reduction in both loads. According to Chen and Teng [40], the bond-controlled strengthening capacity of externally bonded FRP also decreases less than the design equations predict as the compressive strength decreases. Therefore, the contribution of the FRP panel was maintained in deteriorated concrete.

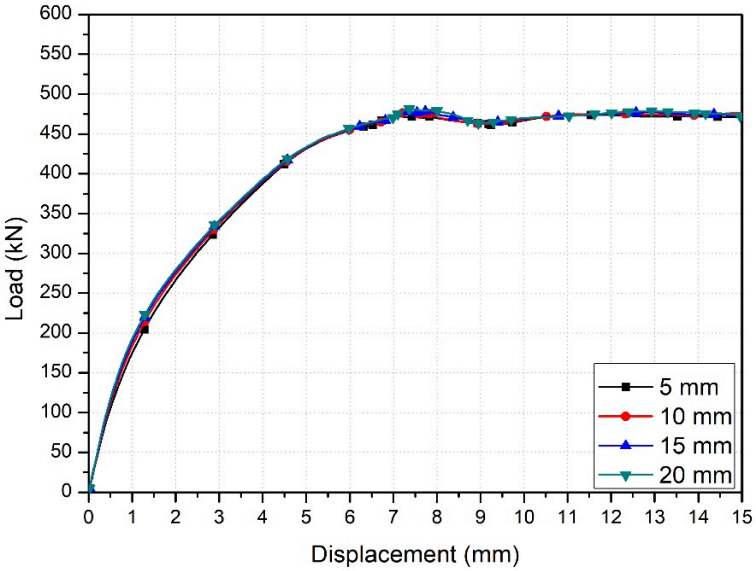


(**a**) Load–displacement relationship

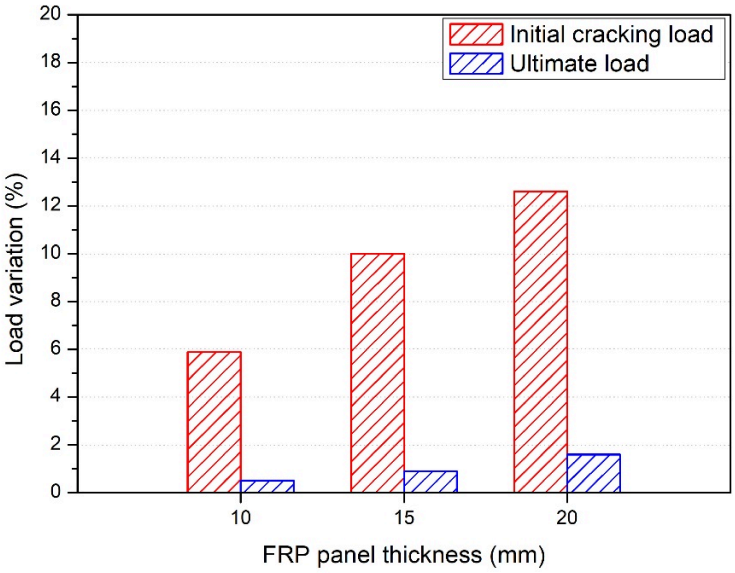


(**b**) Load variation relative to 35 MPa of compressive strength

Figure 14. Analysis results according to concrete compressive strength.



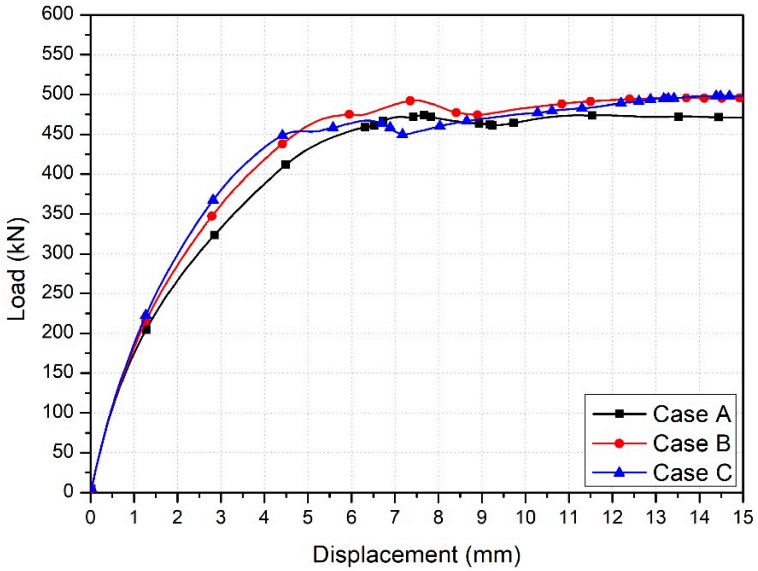
(**a**) Load–displacement relationship



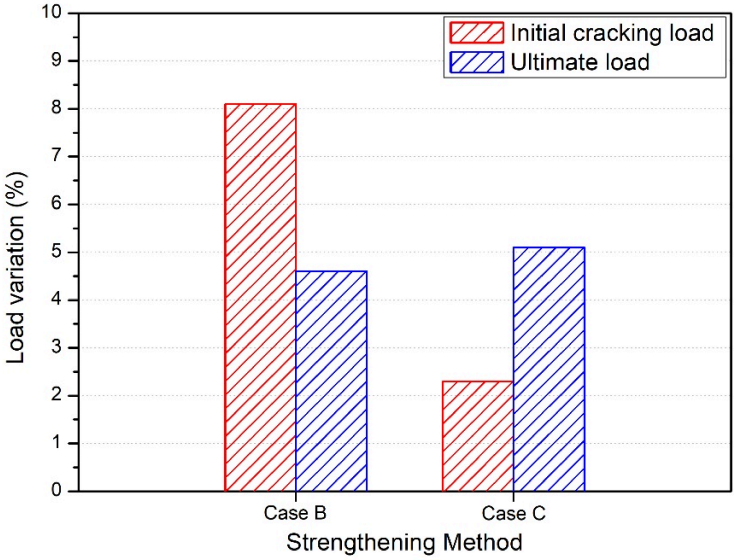
(**b**) Load variation relative to 5 mm of thickness

Figure 15. Analysis results according to FRP panel thickness.

The load–displacement relationships for panel thicknesses from 5 mm to 20 mm in 5 mm steps are presented in Figure 15a. A 20 mm panel gave an initial cracking load 12.6% higher than that of the 5 mm panel. The effect on the ultimate load was limited to 1.6%. Figure 15b presents the load variation relative to the 5 mm panel, which is the gain in each load from the additional thickness. The initial cracking load increased by 5.9%, 10.0%, and 12.6% at 10, 15, and 20 mm (Figure 15b), so the gain from each additional 5 mm became smaller. A thicker panel carries more tension on the inner face of the section and increases the load needed to crack that face. The ultimate load was governed by the diagonal cracking along the compression strut at the slab–haunch junction without the panel, which the thicker panel did not cover. The panel thickness governs the cracking resistance of the box culvert rather than the ultimate load.



(**a**) Load–displacement relationship



(**b**) Load variation relative to case A

Figure 16. Analysis results according to strengthening method.

Figure 16a presents the load–displacement relationships of the three strengthening cases. Figure 16b compares the initial cracking load and the ultimate load of each case with those of case A. Case B increased the initial cracking load by 8.1% and the ultimate load by 4.6%. Relative to case B, case C had 13% more bonded area but increased the ultimate load by 0.4% and decreased the initial cracking load by 5.3%. Case B covered the slab–haunch junction left without the panel in case A, where the critical diagonal crack formed in the strengthened test unit and in the analysis. The panel bonded across the haunch provides an additional tension path around the corner. Case C added bonded area at midspan, where the slab of the reference model remained almost undamaged. A similar increase in bonded area increased the ultimate load by 4.6% when the panel was extended across the haunches (case B) but by 0.4% when the midspan gap was filled (case C). The location of the FRP panel had a greater effect on the ultimate load than the panel thickness or the bonded area.

6. Conclusions

In this study, shear tests were conducted on full-scale precast box culverts with and without bonded FRP strengthening. A three-dimensional nonlinear finite element model based on the concrete damaged plasticity model was constructed and verified. A parametric study was performed on three variables: the concrete compressive strength, the FRP panel thickness, and the strengthening method. The principal conclusions of this study are summarized as follows:

1. Shear strengthening with a 5-mm-thick FRP panel increased the initial cracking load to three times that of the control test unit, from 50 kN to 150 kN. The ultimate load increased by only 0.8% (455.7 kN to 459.2 kN), whereas the deflection at the ultimate load decreased by 50.4% (13.25 mm to 6.57 mm). Therefore, the FRP panel improved the cracking resistance and the stiffness of the box culvert by restraining the tension faces, whereas the ultimate load was governed by the compression strut at the haunch.
2. The yield load of the steel reinforcement in the wall increased by 38% from 300 kN in the control test unit to 414 kN in the strengthened test unit. At about 350 kN, the strain nonlinearity increased in the wall of the control test unit and in the slab of the strengthened test unit. The control test unit failed in the wall, whereas the diagonal crack at the slab–haunch junction without the panel governed the failure of the strengthened test unit without rupture or debonding of the FRP panel. Therefore, the FRP panel delayed the yielding of the wall reinforcement, and the failure moved along the compression strut from the wall to the slab–haunch junction without the panel.
3. The finite element model predicted the initial cracking load and the ultimate load of the strengthened test unit with errors of 2.7% and 3.2%, respectively. The tensile damage concentrated in a diagonal band between the loading area and the haunch, at the location of the critical diagonal crack in the test. Therefore, the model captured the load–displacement behavior and the failure mechanism of the box culvert with bonded FRP strengthening.
4. A reduction in the concrete compressive strength from 35 MPa to 15 MPa decreased the initial cracking load by 25.2% and the ultimate load by 21.5%. Both loads decreased less than the 34.5% reduction predicted by the design equations proportional to $\sqrt{f_{ck}}$. Because the properties of the steel reinforcement and the FRP panel are independent of the compressive strength, these components limited the reduction in both loads. Therefore, the contribution of the FRP panel was maintained in deteriorated concrete.
5. As the panel thickness increased from 5 mm to 20 mm, the initial cracking load increased by 12.6%, whereas the ultimate load increased by only 1.6%. The gain in the initial cracking load from each additional 5 mm decreased as the panel became thicker. Therefore, the panel thickness governs the cracking resistance of the box culvert rather than the ultimate load.
6. Extending the FRP panel across both upper haunches (case B) increased the initial cracking load by 8.1% and the ultimate load by 4.6% relative to the tested arrangement (case A). Case B covered the slab–haunch junction without the panel, where the diagonal crack that governed the failure of the strengthened test unit formed. Filling the midspan gap in addition to the haunches (case C) added 13% more bonded area than case B but increased the ultimate load by only 0.4% and decreased the initial cracking load by 5.3%. Therefore, covering the slab–haunch junction tended to be more effective for the ultimate load than increasing the panel thickness or the bonded area.

This study is limited to one test unit for each condition and to the tested geometry and loading arrangement without soil confinement, which excludes the axial compression induced by the soil pressure in the field. The effects of other culvert dimensions and

the long-term durability of the bond under moisture and temperature changes remain to be examined.

Author Contributions: Conceptualization, T.K., S.C. (Song Choi) and W.C.; methodology, T.K.; validation, S.C. (Sanghyeon Cho); formal analysis, S.C. (Sanghyeon Cho); investigation, T.K. and S.C. (Song Choi); resources, W.C.; data curation, T.K. and S.C. (Song Choi); writing—original draft preparation, T.K.; writing—review and editing, S.C. (Sanghyeon Cho) and W.C.; visualization, T.K. and S.C. (Sanghyeon Cho); supervision, S.C. (Sanghyeon Cho) and W.C.; project administration, W.C.; funding acquisition, W.C. All authors have read and agreed to the published version of the manuscript.

Funding: This research was funded by the National Research Foundation of Korea (NRF) grant funded by the Korean government (MSIT), grant numbers RS-2026-25481667 and RS-2025-25412626.

Institutional Review Board Statement: Not applicable.

Informed Consent Statement: Not applicable.

Data Availability Statement: The data presented in this study are available on request from the corresponding authors because the data are part of an ongoing study.

Acknowledgments: The authors thank Seyeon Inc. Co., Ltd. for supplying the FRP panel and the epoxy resin free of charge and for assisting with the installation of the panel.

Conflicts of Interest: Author Song Choi was employed by the company Seyeon Inc. Co., Ltd., which supplied the FRP panel and the epoxy resin used in this study free of charge and took part in the installation of the panel. The remaining authors declare that the research was conducted in the absence of any commercial or financial relationships that could be construed as a potential conflict of interest. The funders had no role in the design of the study; in the collection, analysis, or interpretation of data; in the writing of the manuscript; or in the decision to publish the results.

References

1. Orton, S.L.; Loehr, J.E.; Boeckmann, A.; Havens, G. Live-Load Effect in Reinforced Concrete Box Culverts under Soil Fill. *J. Bridge Eng.* **2015**, *20*, 04015003. [CrossRef]
2. Tao, Q.; He, Z.; Jia, Y. Influence of Filling Properties and Culvert Structure Parameters on the Soil Arching Effect of Upper-Buried-Type Culverts. *Results Phys.* **2020**, *16*, 103003. [CrossRef]
3. Lee, D.H.; Han, S.J.; Kim, K.S.; LaFave, J.M. Shear Strength of Reinforced Concrete Beams Strengthened in Shear Using Externally-Bonded FRP Composites. *Compos. Struct.* **2017**, *173*, 177–187. [CrossRef]
4. Ferreira, D.; Oller, E.; Marí, A.; Bairán, J. Analysis of FRP Shear Strengthening Solutions for Reinforced Concrete Beams Considering Debonding Failure. *J. Compos. Constr.* **2016**, *20*, 04016018. [CrossRef]
5. Alam, M.A.; Onik, S.A.; Mustapha, K.N.B. Crack Based Bond Strength Model of Externally Bonded Steel Plate and CFRP Laminate to Predict Debonding Failure of Shear Strengthened RC Beams. *J. Build. Eng.* **2020**, *27*, 100943. [CrossRef]
6. Cho, S.; Chung, W.; Jung, W.T.; Park, J.S.; Lee, H. Enhancing the Flexural Capacity of Deteriorated Low-Strength Prestressed Concrete Beam Using Near-Surface Mounted Post-Tensioned Carbon Fiber-Reinforced Polymer Bar. *Int. J. Concr. Struct. Mater.* **2024**, *18*, 58. [CrossRef]
7. Razaqpur, A.G.; Cameron, R.; Mostafa, A.A. Strengthening of RC Beams with Externally Bonded and Anchored Thick CFRP Laminate. *Compos. Struct.* **2020**, *233*, 111574. [CrossRef]
8. Zhang, H.; Smith, S.T. Influence of Plate Length and Anchor Position on FRP-to-Concrete Joints Anchored with FRP Anchors. *Compos. Struct.* **2017**, *159*, 615–624. [CrossRef]
9. Lee, J.; Lopez, M.M. Characterization of FRP U-Wrap Anchors for Externally Bonded FRP-Reinforced Concrete Elements: An Experimental Study. *J. Compos. Constr.* **2016**, *20*, 04016012. [CrossRef]
10. Cho, S.; Chung, W.; Jung, W.T.; Park, J.S.; Lee, H. Assessment of Shear Capacity in NSM Prestressed FRP Strengthening with Anchorage Conditions. *Case Stud. Constr. Mater.* **2024**, *20*, e02743. [CrossRef]
11. Zhang, X.; Wang, X.; Zhang, Y.; Chang, X.; Shi, Y.; Li, G.; Wu, Z. Flexural Behavior of Tunnel Lining Segment Strengthened with BFRP Grid-Fiber Reinforced Geopolymer Mortar. *Structures* **2025**, *74*, 108490. [CrossRef]
12. Zhao, G.; Guo, C.; Wang, F.; He, Y.; Wang, H.; Zhong, J. Experimental Study on the Mechanical Performance of Cracked Tunnel Lining Reinforced with UV-FRP. *Structures* **2025**, *73*, 108294. [CrossRef]

13. Sadat Hosseini, A.; Goill, T.J.; Sadeghian, P. Strengthening Damaged Reinforced Concrete Pipes Using a Novel Sandwich Fiber Composite Liner: Experimental and Numerical Studies. *Structures* **2026**, *86*, 111387. [CrossRef]
14. Wang, S.Q.; Bai, Y.; Gu, H.; Zhao, N.; Cao, X.Y. On-Site Construction and Experimental Study of Prefabricated High-Strength Thin Concrete Segment Liners for the Reinforcement of Underground Box Culverts. *Buildings* **2025**, *15*, 2509. [CrossRef]
15. ACI Committee 440. *Guide for the Design and Construction of Externally Bonded FRP Systems for Strengthening Concrete Structures (ACI 440.2R-17)*; American Concrete Institute: Farmington Hills, MI, USA, 2017.
16. Fédération Internationale du Béton. *Externally Bonded FRP Reinforcement for RC Structures*; Fib Bulletin 14; Fib: Lausanne, Switzerland, 2001. [CrossRef]
17. Garg, A.K.; Abolmaali, A.; Fernandez, R. Experimental Investigation of Shear Capacity of Precast Reinforced Concrete Box Culverts. *J. Bridge Eng.* **2007**, *12*, 511–517. [CrossRef]
18. Ghahremannejad, M.; Abolmaali, A. Shear Capacity of Reinforced Concrete Box Culverts Compared with AASHTO Shear Equation. *J. Bridge Eng.* **2019**, *24*, 04019032. [CrossRef]
19. Waqas, H.A.; Waseem, M.; Riaz, A.; Ilyas, M.; Naveed, M.; Seitz, H. Influence of Haunch Geometry and Additional Steel Reinforcement on Load Carrying Capacity of Reinforced Concrete Box Culvert. *Materials* **2023**, *16*, 1409. [CrossRef] [PubMed]
20. Elnady, A.; Mousa, S.; Benmokrane, B. Two-Way Shear Strength of GFRP-Reinforced Precast Concrete Box Culverts under Vertical Concentrated Loading. *J. Compos. Constr.* **2025**, *29*, 04024085. [CrossRef]
21. He, C.; Wu, H.; Huang, S.; Li, J.; Ma, B. Glass Reinforced Plastic (GRP) Liner-Enhanced Load-Bearing Performance of Reinforced Concrete Box Culverts: Experimental and Numerical Investigation. *Constr. Build. Mater.* **2025**, *498*, 144023. [CrossRef]
22. Ejaz, M.F.; Komatsu, S.; Kawamura, K.; Matsuo, T. Shear Behavior of Pre-Damaged RC Members with Post Installed Headed Shear Reinforcements under Dynamic Loading: Novel Experimental Insights in Air and Submerged Conditions. *Constr. Build. Mater.* **2025**, *498*, 144032. [CrossRef]
23. Cho, S.; Choi, J.; Lee, H.; Chung, W. Structural Behavior of Construction Joints in a Composite Rigid-Frame Bridge. *Int. J. Concr. Struct. Mater.* **2023**, *17*, 54. [CrossRef]
24. ACI Committee 318. *Building Code Requirements for Structural Concrete (ACI 318-19) and Commentary*; American Concrete Institute: Farmington Hills, MI, USA, 2019.
25. Dassault Systèmes. *ABAQUS 2022 Analysis User's Guide*; Dassault Systèmes Simulia Corp.: Providence, RI, USA, 2022.
26. Genikomsou, A.S.; Polak, M.A. Finite Element Analysis of Punching Shear of Concrete Slabs Using Damaged Plasticity Model in ABAQUS. *Eng. Struct.* **2015**, *98*, 38–48. [CrossRef]
27. Seręga, S.; Kotynia, R. Numerical Modeling of RC Beams Strengthened with Non-Pretensioned and Pretensioned NSM CFRP Strips. *Materials* **2026**, *19*, 2357. [CrossRef] [PubMed]
28. Lubliner, J.; Oliver, J.; Oller, S.; Oñate, E. A Plastic-Damage Model for Concrete. *Int. J. Solids Struct.* **1989**, *25*, 299–326. [CrossRef]
29. Lee, J.; Fenves, G.L. Plastic-Damage Model for Cyclic Loading of Concrete Structures. *J. Eng. Mech.* **1998**, *124*, 892–900. [CrossRef]
30. Mander, J.B.; Priestley, M.J.N.; Park, R. Theoretical Stress-Strain Model for Confined Concrete. *J. Struct. Eng.* **1988**, *114*, 1804–1826. [CrossRef]
31. Hordijk, D.A.; Reinhardt, H.W. Fracture of Concrete in Uniaxial Tensile Experiments as Influenced by Curing Conditions. *Eng. Fract. Mech.* **1990**, *35*, 819–826. [CrossRef]
32. Bažant, Z.P.; Oh, B.H. Crack Band Theory for Fracture of Concrete. *Mater. Struct.* **1983**, *16*, 155–177. [CrossRef]
33. Hillerborg, A.; Modéer, M.; Petersson, P.E. Analysis of Crack Formation and Crack Growth in Concrete by Means of Fracture Mechanics and Finite Elements. *Cem. Concr. Res.* **1976**, *6*, 773–781. [CrossRef]
34. Comité Euro-International du Béton. *CEB-FIP Model Code 1990*; Thomas Telford: London, UK, 1993. [CrossRef]
35. Fédération Internationale du Béton. *Fib Model Code for Concrete Structures 2010*; Ernst & Sohn: Berlin, Germany, 2013. [CrossRef]
36. Alfarah, B.; López-Almansa, F.; Oller, S. New Methodology for Calculating Damage Variables Evolution in Plastic Damage Model for RC Structures. *Eng. Struct.* **2017**, *132*, 70–86. [CrossRef]
37. Kmiecik, P.; Kamiński, M. Modelling of Reinforced Concrete Structures and Composite Structures with Concrete Strength Degradation Taken into Consideration. *Arch. Civ. Mech. Eng.* **2011**, *11*, 623–636. [CrossRef]
38. Jankowiak, T.; Łodygowski, T. Identification of Parameters of Concrete Damage Plasticity Constitutive Model. *Found. Civ. Environ. Eng.* **2005**, *6*, 53–69.
39. Lu, X.Z.; Teng, J.G.; Ye, L.P.; Jiang, J.J. Bond-Slip Models for FRP Sheets/Plates Bonded to Concrete. *Eng. Struct.* **2005**, *27*, 920–937. [CrossRef]
40. Chen, J.F.; Teng, J.G. Anchorage Strength Models for FRP and Steel Plates Bonded to Concrete. *J. Struct. Eng.* **2001**, *127*, 784–791. [CrossRef]

Disclaimer/Publisher's Note: The statements, opinions and data contained in all publications are solely those of the individual author(s) and contributor(s) and not of MDPI and/or the editor(s). MDPI and/or the editor(s) disclaim responsibility for any injury to people or property resulting from any ideas, methods, instructions or products referred to in the content.